

Submolecular-scale imaging of α -helices and C-terminal domains of tubulins by frequency modulation atomic force microscopy in liquid

メタデータ	言語: eng 出版者: 公開日: 2017-10-06 キーワード (Ja): キーワード (En): 作成者: メールアドレス: 所属:
URL	https://doi.org/10.24517/00039989

This work is licensed under a Creative Commons Attribution-NonCommercial-ShareAlike 3.0 International License.



Submolecular-scale Imaging of α -Helices and C-Terminal Domains of Tubulins by Frequency Modulation Atomic Force Microscopy in Liquid

Hitoshi Asakawa
Bio-AFM Frontier Research Center,
Kanazawa University, Kanazawa, Ishikawa 920-1192, Japan

Koji Ikegami and Mitsutoshi Setou
Department of Molecular Anatomy,
Hamamatsu University School of Medicine,
Hamamatsu, Shizuoka 431-3192, Japan

Naoki Watanabe
Mizuho Information & Research Institute, Inc.,
Chiyoda-ku, Tokyo 101-8443, Japan

Masaru Tsukada
WPI Advanced Institute for Materials Research,
Tohoku University, Aobaku, Sendai 980-8577, Japan

Takeshi Fukuma *
Frontier Science Organization
and Bio-AFM Frontier Research Center,
Kanazawa University, Kanazawa, Ishikawa 920-1192, Japan
PRESTO,
Japan Science and Technology Agency, Honcho 4-1-9, Kawaguchi 332-0012, Japan

July 20, 2011

*Corresponding author. Address: Frontier Science Organization, Kanazawa University, Kakuma-machi, Kanazawa, Ishikawa 920-1192, Japan, Tel.: +81(76)234-4847, Fax: +81(76)234-4632

Abstract

In this study, we have performed the direct imaging of subnanometer-scale structures of tubulins by frequency modulation atomic force microscopy (FM-AFM) in liquid. Individual α -helices at the surface of a tubulin protofilament are imaged as periodic corrugations with a spacing of 0.53 nm, which corresponds to the common pitch of an α -helix backbone (0.54 nm). The identification of individual α -helices allowed us to determine the orientation of the deposited tubulin protofilament. As a result, C-terminal domains of tubulins are identified as protrusions with a height of 0.4 nm from the surface of the tubulin. The imaging mechanism for the observed subnanometer-scale contrasts is discussed in relation to the possible structures of the C-terminal domains. As the C-terminal domains are chemically modified to regulate the interactions between tubulins and other biomolecules [e.g., motor proteins and microtubule-associated proteins (MAPs)], detailed structural information on individual C-terminal domains is valuable for understanding such regulation mechanisms. The results obtained in this study demonstrate that FM-AFM is capable of visualizing the structural variation of tubulins with subnanometer resolution. This is an important first step towards the use of FM-AFM for such analysis of the functions of tubulins.

Key words: frequency modulation atomic force microscopy; FM-AFM; tubulin; α -helix; C-terminal domain

Introduction

X-ray and electron crystallography are well-established techniques for the structural analysis of proteins with atomic-scale resolution. For example, Nogales and coworkers determined the atomic-scale structure of an $\alpha\beta$ -tubulin heterodimer in a Zn-sheet structure by electron crystallography (1, 2). Subsequently, Gigant et al. investigated the structure of tubulin complexes with stathmin-like domains by X-ray crystallography (3). NMR, electron microscopy (EM) and electron tomography (ET) have also been used to visualize protein structures with Ångstrom resolution. For example, Sosa et al. and Kikkawa et al. investigated the binding structures of motor proteins on the surface of tubulins by cryo-EM (4, 5). In addition, Sui and Downing visualized the doublet structures of tubulin microtubules by cryo-ET (6).

Atomic force microscopy (AFM) (7, 8) has also been an important tool for investigating of the surface structures of proteins. AFM has some advantages in the structural analysis of proteins. For example, AFM imaging does not require the chemical modification of a sample, such as by staining or isotopic modification. Moreover, it can be operated in solution. Therefore, various proteins have been investigated by AFM with nanometer and subnanometer resolution. Contact-mode (CM-) AFM has been used to investigate various protein structures including not only purified proteins but also native membrane proteins (9–15). For example, Karrasch et al. reported CM-AFM images of intermediate filaments and bacteriophages that were covalently fixed on glass substrates (11). Among the studies on the membrane proteins, Müller and coworkers imaged the structural changes (16) and flexibilities (17) of a bacteriorhodopsin with subnanometer resolution. Hoh et al. investigated individual connexons of gap junctions in native membranes isolated from a rat liver (10). These CM-AFM studies in liquids have allowed us to determine the functional structures of proteins in their natural environment and the structural changes at work (18).

One of the drawbacks of CM-AFM is that it cannot be used for imaging isolated biomolecular structures weakly attached to a substrate owing to the influence of the lateral friction force during imaging. To overcome this problem, amplitude modulation (AM-) AFM has been used (19, 20). The lateral friction force is dramatically reduced by oscillating a cantilever at its resonance frequency in AM-AFM. Using AM-AFM in liquid, a variety of isolated proteins have been investigated. For example, Kasas et al. used AM-AFM to investigate the molecular-scale structures of RNA polymerases and their activity to produce RNAs from nucleotides on mica (21). The results demonstrated the capability of AM-AFM to monitor the biological activities of proteins that are weakly attached to a substrate. As another example, Möller et al. reported AM-AFM images of purple membranes

and hexagonally packed intermediate (HPI) layers to demonstrate the capability of AM-AFM for the subnanometer-scale imaging of proteins in a liquid (22). Many other applications of CM- and AM-AFM in protein analyses have been thoroughly reviewed in (23–25). In addition to the large number of biological applications of CM- and AM-AFM, novel imaging modes of AFM (e.g., bimodal AFM (26, 27) and jumping-mode AFM (28)) have also been developed to improve the performance of AFM techniques.

These previous studies have shown the capability of AFM to analyze the structures and mechanical properties of proteins with subnanometer resolution in liquid. However, it is often difficult to assign a submolecular-scale contrast to a specific structure of a protein when the orientation of the deposited protein is unknown. Therefore, the orientation of randomly deposited proteins must be determined for submolecular-scale investigations of proteins by AFM. To determine the orientation of proteins by AFM, it is necessary to specify structural features such as secondary structures at the surfaces of proteins.

Recent progress in frequency modulation AFM (FM-AFM) (29) has made it possible to perform true atomic-resolution imaging in liquid with piconewton-order loading forces (30, 31). In addition, the applicability of FM-AFM to biological studies has been demonstrated by imaging molecular- and submolecular-scale structures of various biological systems (32–37). Hoogenboom and coworkers have investigated membrane proteins [e.g., bacteriorhodopsin (32) and voltage-dependent anion channels (38)] in native membranes by FM-AFM in liquid. In addition, Fukuma et al. imaged individual β -strands constituting an isolated amyloid fibril deposited on a mica surface (34). This result demonstrated the unique capability of FM-AFM to visualize secondary structures of proteins.

Tubulins are globular proteins with a diameter of approximately 4 nm (1). The $\alpha\beta$ -tubulin heterodimer is known as a common building block of microtubules, which are one of the cytoskeletons and have a diameter of 25 nm. Microtubules serve as structural components within cells and are involved in many cellular processes. For example, microtubules act as a molecular rail for motor proteins such as kinesin and dynein in intracellular transportation. Previous studies have suggested that such cellular functions of tubulin microtubules are regulated by post-translational modifications of the C-terminal domains of tubulins (39–41). In spite of their importance, the detailed conformation of tubulin C-terminal domains and its relation to their functions have not been clarified, even by well-established techniques such as X-ray crystallography and NMR. Although this has been ascribed to the local variations or fluctuations of tubulin C-terminal domains, direct evidence for either of the models has yet to be presented.

AFM has been used for the investigation of microtubules and other

tubulin structures such as protofilaments. Fritz et al. and other groups have investigated the surface structures and elasticity of microtubules by AFM in liquid (20, 42, 43). In addition, Elie-Caille et al. reported the AM-AFM imaging of tubulin protofilaments to reveal the effect of paclitaxel (taxol) on molecular arrangements (44). The previous study by Elie-Caille et al. showed that molecular-scale structures and their arrangements in tubulin protofilaments can be quantitatively analyzed by AM-AFM in liquid.

In this study, we have investigated the surface structures of tubulins by FM-AFM in liquid to show the applicability of FM-AFM for the identification of subnanometer-scale structures at the surfaces of tubulins. On the basis of the submolecular-scale AFM images of tubulin protofilaments, we discuss the arrangement of α -helices and C-terminal domains at the surface of tubulins.

Materials and Methods

Sample preparation

The tubulins used in this study were purified from pig brains through two cycles of polymerization-depolymerization and phosphocellulose column chromatography (45). The stock solution of the tubulins was diluted with buffer solution to a concentration of 1 mg ml^{-1} . In this study, two types of buffer solution were used to prepare tubulin protofilaments and sheet-like structures. PEM-G buffer solution (80 mM PIPES, 1 mM MgCl_2 , 1 mM EGTA, 1 mM GTP, pH 6.8) was used for the preparation of tubulin protofilaments. In the imaging of tubulin sheet-like structures, MES-Zn buffer solution (140 mM MES, 0.7 mM MgCl_2 , 0.3 mM EGTA, 1 mM GTP, 0.7 mM ZnCl_2 , pH 5.8) was used. The tubulin solution (1 mg ml^{-1}) was incubated at 37°C for 30 min to form tubulin protofilaments or sheet-like structures by polymerization. After the addition of $10 \text{ }\mu\text{M}$ taxol, the solution was ultracentrifuged at 37°C and $87,000 \times g$ for 10 min. The precipitate was depolymerized by incubation at 4°C for 1 h followed by sedimentation. The supernatant was incubated at 37°C for 30 min, then the tubulin structures were stabilized by the addition of $10 \text{ }\mu\text{M}$ taxol.

For FM-AFM imaging, tubulin solution ($200 \text{ }\mu\text{l}$) was deposited onto a freshly cleaved mica surface (ϕ 12 mm). The sample was incubated at room temperature (25°C) for 30 min and rinsed with PEM-G or MES-Zn buffer solution for the preparation of protofilaments or sheet-like structures, respectively.

The size distribution of tubulin structures in the buffer solution was analyzed using a laser diffraction particle size analyzer (ELSZ-2, Otsuka Electron, Japan). The system can detect particles with sizes

from 0.6 nm to 7 μm , which is sufficient to identify types of tubulin structures such as heterodimers, protofilaments and microtubules. The tubulin solution was maintained at 37°C in a disposable plastic cell during the measurement of the size distribution.

FM-AFM imaging

AFM measurements were performed using a home-built ultralow-noise FM-AFM (30) combined with a commercially available AFM controller (RC-4, Nanonis, Switzerland). All AFM experiments were performed at room temperature (25°C) in PEM-G buffer solution or MES-Zn buffer solution. A commercially available silicon cantilever (PPP-NCH, Nanoworld, Switzerland) with a nominal spring constant of 42 N m⁻¹ and a resonance frequency of 150 kHz in liquid was used. A phase-locked loop (PLL) circuit (OC-4, Nanonis, Switzerland) was used to detect the frequency shift as well as to oscillate the cantilever at its resonance frequency with a constant amplitude.

Results and Discussion

Molecular-scale imaging of tubulin protofilaments

Fig. 1(a) shows the size distribution of tubulin structures in the tubulin solution measured by the dynamic light scattering method. Peak (i) at 9.1 nm corresponds to the length of a single $\alpha\beta$ -tubulin heterodimer. In the microtubule formation, $\alpha\beta$ -tubulin heterodimers form a linear repeating structure with a head-to-tail arrangement, which is known as a tubulin protofilament. 13-15 protofilaments are aligned in parallel to form a microtubule with a cylindrical structure *in vivo* and *in vitro*. The existence of peak (ii) at 165 nm and peak (iii) at 1,128 nm suggests that the tubulin solution contains at least two other types of tubulin structures, which are probably protofilaments and microtubules.

Fig. 1(b) shows an FM-AFM image of tubulin structures deposited on a cleaved mica using the same tubulin solution, which contains $\alpha\beta$ -heterodimers, protofilaments and microtubules. A number of fibrillar structures with a length from 30 to 200 nm are found in the AFM image. The width of the fibrillar structures (approximately 9.9 nm) is smaller than the diameter of a microtubule (25 nm). According to previous AM-AFM studies by Elie-Caille et al. and another group (44, 46), tubulin protofilaments are adsorbed on cleaved mica without surface modification. In contrast, other previous studies reported that microtubules are not readily attached to negatively charged surfaces, such as mica and glass, owing to electrostatic repulsion between the negatively charged microtubule surfaces and the negatively charged substrate (20, 47). Thus, the tubulin structures found in the AFM image

are mostly tubulin protofilaments, although the solution contains other tubulin structures.

Figs. 2(a) and 2(b) show an FM-AFM image of an isolated tubulin protofilament on mica and the model of a protofilament consisting of three $\alpha\beta$ -tubulin heterodimers, respectively. The height profiles along lines A-B and C-D in Fig. 2(a) are respectively shown in Figs. 2(c) and 2(d). As indicated by arrows in Figs. 2(a) and 2(d), the surface of the protofilament exhibits a periodic corrugation with a periodicity of approximately 4 nm, in agreement with the diameter of a tubulin monomer. The average spacing of 4 nm also shows good agreement with previously reported results obtained by AM-AFM and EM (44, 48). In addition, the height of the protofilament is also 4 nm, as shown in Fig. 2(c). In contrast, the apparent width of the protofilament in the FM-AFM image is 9.9 nm [as shown in Fig. 2(c)], which is more than two times larger than the actual diameter of a protofilament (approximately 4 nm). This increase in the width of the fibrillar structure can be explained by the effect of the nanoscale tip geometry (49). Thus, these results demonstrate that individual tubulins constituting a protofilament can directly be imaged by FM-AFM in a physiologically relevant solution.

In this experiment, we were not able to obtain a submolecular-scale FM-AFM image of an isolated protofilament, although we endeavored to optimize the imaging parameters such as the amplitude of cantilever vibration (A), the frequency shift (Δf) and the tip velocity (v) to improve the resolution of the image. In addition, we often observed the dissociation of tubulins from a protofilament during the imaging. In their previous study, Elie-Caille et al. reported the stable high-resolution imaging of protofilaments deposited on mica by AM-AFM using cantilevers with $k=0.3$ and 0.6 N m^{-1} (44). However, such stable high-resolution imaging of protofilaments was difficult in this experiment. This may be because we used a relatively stiff cantilever ($k=42 \text{ N m}^{-1}$), and hence a transient feedback error may cause a large loading force to be applied to the sample. Although the rigidity of a protofilament can be increased by chemical modification to bridge adjacent tubulins using linker molecules, submolecular-scale features of its surface are also likely to be modified. Therefore, such chemical modification is not desirable for submolecular-scale AFM studies.

Submolecular-scale imaging of tubulin sheet-like structures

Fig. 3(a) shows FM-AFM images of tubulin protofilaments prepared with MES-Zn buffer solution. As previously reported (1, 50, 51), tubulins form Zn-sheet structures in MES-Zn buffer solution. Zn ions are known to bridge tubulin protofilaments and help form a large Zn-

sheet structure. However, in this experiment, we found small sheet-like structures in which protofilaments are aligned in parallel as shown in Fig. 3(b). Fig. 3(c) shows a height profile measured along the axis of a protofilament [line A-B in Fig. 3(b)]. The profile shows a periodic corrugation with a spacing of approximately 4 nm, which agrees with that of an isolated protofilament [see Fig. 2(a)]. Although the tubulin structures observed in the large-scale AFM image [Fig. 3(a)] look similar to the protofilaments in Fig. 1(b), we found a difference between them in high-resolution AFM images with a small scanning size [Fig. 3(b)]. In this study, we could not observe subnanometer-scale contrasts at the surface of protofilaments prepared with PEM-G buffer solution, whereas it was possible to be observed on the sheet-like structures prepared with MES-Zn buffer solution. As described above, it is likely that the submolecular-scale imaging of isolated protofilaments was hindered by the high loading force resulting from the use of a stiff cantilever. Therefore, we speculate that the subnanometer-scale imaging of the protofilaments in the sheet-like structures was possible because of the stabilization by Zn ions bridging adjacent protofilaments.

A part of Fig. 3(b) is magnified in Fig. 3(d) to highlight the detailed subnanometer-scale contrasts observed on the tubulin sheet-like structure. The length of the scale bar in Fig. 3(d) corresponds to the diameter of a tubulin (4 nm). In this experiment, we used cantilever vibration with a very small oscillation amplitude ($A < 0.5$ nm) to enhance the sensitivity of the frequency shift signal to the short-range interaction forces acting between the front atoms of the tip and the sample. Thus, subnanometer-resolution images can be obtained even with a tip diameter of a few nanometers. The image shown in Fig. 3(d) demonstrates that subnanometer-scale structures within individual tubulins can be visualized by FM-AFM. The observed subnanometer-scale contrasts show a large variation. We speculate that this is caused by the difference in the rotational orientation of the protofilaments.

Although we were not able to assign all the subnanometer-scale contrasts to a specific tubulin structure, this was possible in some cases, as shown in Fig. 4(a), where the rotational orientation was determined from the AFM image. In Fig. 4(a), one of the protofilaments constituting the tubulin sheet-like structure was imaged with a smaller scan size. The image shows nanoscale repeating structures corresponding to the tubulin monomers as well as subnanometer-scale features within each molecule. In particular, the fine features indicated by the arrows in Fig. 4(a) exhibit a periodic corrugation with a spacing of 0.53 nm, as revealed by a cross-sectional plot taken along line A-B (Fig. 4(b)). This average spacing is in agreement with the common pitch of an α -helix backbone (0.54 nm), as illustrated in Fig. 4(c), which strongly suggests that the periodic features correspond to α -helices at the tubulin surface.

An important finding here is that the backbones of α -helices can be imaged by FM-AFM with clear contrasts, even though the backbones are buried under fluctuating side chains. This result can be explained by the rigidity of an α -helix backbone. In general, an α -helix backbone is stabilized by 3-4 parallel hydrogen bonds per turn. Thus, a backbone with a helical structure is more rigid than the fluctuating side chains. Therefore, the interaction between the tip and the α -helix backbone may predominantly contribute to the formation of the image contrasts, whereas the interaction between the tip and the side chains may be smeared out by their random motion, leading to almost no image contrast.

The direct imaging of α -helices provides useful information for identifying the orientation of a tubulin protofilament. Although the structural model of a tubulin protofilament is known, interpretation of the subnanometer-scale features in the FM-AFM image require the determination of the rotation angle of the protofilament. The subnanometer-resolution FM-AFM image [Fig. 4(a)] was compared with the known structural model of the tubulin heterodimer (PDB ID: 1JFF) with various rotation angles. As a result, we found that the arrangement of the observed α -helices exhibits greatest agreement with that of the structural model when the rotation angle is set as shown in Fig. 4(d). The red regions of the structural model represent α -helices at the surface of tubulins. Although it is difficult to distinguish between α - and β -tubulins in the FM-AFM image, the result allowed us to determine the directions of (+) and (-) ends in the tubulin protofilament as shown in Fig. 4(a).

Moreover, the good agreement between the AFM image and the structural model allowed us to interpret local features in the high-resolution FM-AFM image. The positions of the bright protrusions observed in the FM-AFM image [Fig. 4(a)] agreed with those of the C-terminal domains in the structural model [Fig. 4(d)]. This result demonstrates that the C-terminal domains of tubulins can be directly imaged by FM-AFM in liquid.

To enhance the contrast of the bright protrusions, the color scale of the AFM image was adjusted as shown in Fig. 5(a). In addition, the same FM-AFM image is shown with a 21-step color scale in Fig. 5(b) for comparison of the subnanometer-scale structures within the C-terminal domains between different molecules. The AFM image shows that the bright protrusions have similar oval shapes with lengths of the longer and shorter axes of 2-3 and 1-2 nm, respectively. The height of the protrusions is almost uniform and is approximately 0.4 nm from the surface of the tubulins. However, small corrugations within the C-terminal domains exhibit variation depending on the molecules as shown in Fig. 5(b). The results demonstrate the capability of FM-AFM to visualize structural differences between different C-terminal

domains with subnanometer-scale resolution.

According to previous studies (52–54), a C-terminal domain of a tubulin consists of approximately 10–25 residues and has a variation in length and constituent amino acids owing to the existence of different isotypes. In one of the structural models (54, 55), the C-terminal domain is considered to protrude from the tubulin surface a few nanometers into the solution with significant fluctuations. Although the height of the protrusions in the AFM image (0.4 nm) is lower than the expected height of the C-terminal domain in the extended form, the tip may be scanned over the fixed end of the C-terminal domain during the AFM imaging as shown in Fig. 5(c).

In contrast, previous NMR studies using a synthetic short peptide as a model of a C-terminal domain suggested that the peptide model has a relatively compact structure under a low pH condition (pH 5) owing to the helical conformation formed by the several residues (55). Since the subnanometer-scale FM-AFM image [Fig. 4(a)] was obtained under a slightly acidic condition (MES-Zn buffer, pH 5.8), there is a possibility that the C-terminal domains were taking a folded structure as illustrated in Fig. 5(d).

Previous studies on microtubules showed that the polyglutamylation of C-terminal domains at the surfaces of tubulins affects the binding of kinesins and MAPs to microtubules (39, 56–58). These molecular interactions play an important role in the major functions of microtubules such as intracellular transport and cell division. To understand the mechanisms of these functions in detail, submolecular-scale changes at the surface of tubulins caused by chemical modification need to be investigated. The results obtained in this study demonstrate that FM-AFM allows us to visualize subnanometer-scale structures of tubulins. This capability should be of considerable use in future studies on the molecular-scale mechanisms of tubulin functions.

Conclusions

We have demonstrated the molecular- and submolecular-scale imaging of tubulins by FM-AFM in liquid. In the imaging of tubulin protofilaments, individual tubulins were clearly imaged by FM-AFM. The result shows the applicability of FM-AFM to the molecular-resolution imaging of isolated tubulin protofilaments. In the imaging of tubulin sheet-like structures, the individual α -helices were imaged as a periodic contrast with a spacing corresponding to the pitch of an α -helix backbone. This is the first demonstration of the real-space imaging of individual α -helices in liquid. By determining the position of the α -helices, we were able to identify the orientation of tubulins. As a result, we found that the C-terminal domains are imaged by FM-AFM

as bright protrusions with a height of 0.4 nm. These results obtained in this study demonstrate that FM-AFM is capable of identifying arrangements of secondary structures such as α -helices and C-terminal domains at the tubulin surface. This capability should be of considerable use in future studies on the molecular-scale mechanisms of tubulin functions.

Acknowledgements

The authors thank T. Hayasaka (Hamamatsu University School of Medicine) for his help in the preparation of the tubulin samples.

This work was supported by PRESTO, Japan Science and Technology Agency.

References

1. Nogales, E., S. G. Wolf, and K. H. Downing, 1998. Structure of the $\alpha\beta$ tubulin dimer by electron crystallography. *Nature* 391:199–202.
2. Löwe, J., K. H. Downing, and E. Nogales, 2001. Refined structure of $\alpha\beta$ -tubulin at 3.5 Å resolution. *J. Mol. Biol.* 313:1045–1057.
3. Gigant, B., P. A. Curmi, C. Martin-Barbey, E. Charbaut, S. Lachkar, L. Lebeau, S. Siavoshian, A. Sobel, and M. Knossow, 2000. The 4 Ångstrom X-ray structure of a tubulin:stathmin-like domain complex. *Cell* 102:809–816.
4. Sosa, H., D. P. Dias, A. Hoenger, M. Whittaker, E. Wilson-Kubalek, E. Sablin, R. J. Fletterick, R. D. Vale, and R. A. Milligan, 1997. A model for the microtubule-Ncd motor protein complex obtained by cryo-electron microscopy and image analysis. *Cell* 90:217–224.
5. Kikkawa, M., Y. Okada, and N. Hirokawa, 2000. 15 Å resolution model of the monomeric kinesin motor, KIF1A. *Cell* 100:241–252.
6. Sui, H., and K. H. Downing, 2006. Molecular architecture of axonemal microtubule doublets revealed by cryo-electron tomography. *Nature* 442:475–478.
7. Binnig, G., C. F. Quate, and C. Gerber, 1986. Atomic force microscope. *Phys. Rev. Lett.* 56:930–933.
8. Giessibl, F. J., 2003. Advances in atomic force microscopy. *Reviews of Modern Physics* 75:949–983.

9. Drake, B., C. B. Prater, A. L. Weisenhorn, S. A. C. Gould, T. R. Albrecht, C. F. Quate, D. S. Cannell, H. G. Hansma, and P. K. Hansma, 1989. Imaging crystals, polymers, and processes in water with the atomic force microscopy. *Science* 243:1586–1588.
10. Hoh, J. H., G. E. Sosinsky, J. P. Revel, and P. K. Hansma, 1993. Structure of the extracellular surface of the gap junction by atomic force microscopy. *Biophys. J.* 65:149–163.
11. Karrasch, S., M. Dolder, F. Schabert, J. Ramsden, and A. Engel, 1993. Covalent binding of biological samples to solid supports for scanning probe microscopy in buffer solution. *Biophys. J.* 65:2437–2446.
12. Karrasch, S., R. Hegerl, J. H. Hoh, W. Baumeister, and A. Engel, 1994. Atomic force microscopy produces faithful high-resolution images of protein surfaces in an aqueous environment. *Proc. Natl. Acad. Sci. USA* 91:836–838.
13. Yang, J., J. Mou, and Z. Shao, 1994. Molecular resolution atomic force microscopy of soluble proteins in solution. *Biochim. Biophys. Acta* 1199:105–114.
14. Schabert, F. A., C. Henn, and A. Engel, 1995. Native Escherichia coli OmpF porin surfaces probed by atomic force microscopy. *Science* 268:92–94.
15. Müller, D. J., D. Fotiadis, S. Scheuring, S. A. Müller, and A. Engel, 1999. Electrostatically balanced subnanometer imaging of biological specimens by atomic force microscopy. *Biophys. J.* 76:1101–1111.
16. Müller, D. J., F. A. Schabert, G. Büldt, and A. Engel, 1995. Imaging purple membranes in aqueous solutions at sub-nanometer resolution by atomic force microscopy. *Biophys. J.* 68:1681–1686.
17. Müller, D. J., D. Fotiadis, and A. Engel, 1998. Mapping flexible protein domains at subnanometer resolution with the atomic force microscopy. *FEBS Lett.* 430:105–111.
18. Frederix, P., T. Akiyama, S. Staufer, C. Gerber, D. Fotiadis, D. Muller, and A. Engel, 2003. Atomic force bio-analytics. *Curr. Opin. Chem. Biol.* 265:641–647.
19. Hansma, P. K., J. P. Cleveland, M. Radmacher, D. A. Walters, P. E. Hillner, M. Bezanilla, M. Fritz, D. Vie, H. G. Hansma, C. B. Prater, J. Massie, L. Fukunaga, J. Gurley, and V. Elings, 1994. Tapping mode atomic force microscopy in liquids. *Appl. Phys. Lett.* 64:1738–1740.

20. Fritz, M., M. Radmacher, J. P. Cleveland, M. W. Allersma, R. J. Stewart, R. Gieselmann, P. Janmey, C. F. Schmidt, and P. K. Hansma, 1995. Imaging globular and filamentous proteins in physiological buffer solutions with tapping mode atomic force microscopy. *Langmuir* 11:3529–3535.
21. Kasas, S., N. H. Thomson, B. L. Smith, H. G. Hansma, X. Zhu, M. Guthold, C. Bustamante, E. T. Kool, M. Kashlev, and P. K. Hansma, 1997. Escherichia coli RNA polymerase activity observed using atomic force microscopy. *Biochemistry* 36:461–468.
22. Möller, C., M. Allen, V. Elings, A. Engel, and D. J. Müller, 1999. Tapping-mode atomic force microscopy produces faithful high-resolution images of protein surfaces. *Biophys. J.* 77:1150–1158.
23. Müller, D. J., H. Janovjak, T. Lehto, L. Kuerschner, and K. Anderson, 2002. Observing structure, function and assembly of single proteins. *Prog. Biophys. Mol. Biol.* 79:1–43.
24. Kada, G., F. Kienberger, and P. Hinterdorfer, 2008. Atomic force microscopy in bionanotechnology. *Nanotoday* 3:12–19.
25. Müller, D. J., and Y. F. Dufrene, 2008. Atomic force microscopy as a multifunctional molecular toolbox in nanobiotechnology. *Nat. Nanotec.* 3:261–269.
26. Martínez, N. F., J. R. Lozano, E. T. Herruzo, F. Garcia, C. Richter, T. Sulzbach, and R. Garcia, 2008. Bimodal atomic force microscopy imaging of isolated antibodies in air and liquids. *Nanotechnology* 19:384011–384018.
27. Martinez-Martin, D., E. T. Herruzo, C. Dietz, J. Gomez-Herrero, and R. Garcia, 2011. Noninvasive protein structural flexibility mapping by bimodal dynamic force microscopy. *Phys. Rev. Lett.* 106:198101–198104.
28. Moreno-Herrero, F., J. Colchero, J. Gómez-Herrero, and A. M. Baró, 2004. Atomic force microscopy contact, tapping, and jumping modes for imaging biological samples in liquids. *Phys. Rev. E* 69:31915–31923.
29. Albrecht, T. R., P. Grütter, D. Horne, and D. Rugar, 1991. Frequency modulation detection using high-Q cantilevers for enhanced force microscope sensitivity. *J. Appl. Phys.* 69:668–673.

30. Fukuma, T., M. Kimura, K. Kobayashi, K. Matsushige, and H. Yamada, 2005. Development of low noise cantilever deflection sensor for multienvironment frequency-modulation atomic force microscopy. *Rev. Sci. Instrum.* 76:053704–053711.
31. Fukuma, T., K. Kobayashi, K. Matsushige, and H. Yamada, 2005. True atomic resolution in liquid by frequency-modulation atomic force microscopy. *Appl. Phys. Lett.* 87:034101–034103.
32. Hoogenboom, B. W., H. J. Hug, Y. Pellmont, S. Martin, P. L. T. M. Frederix, D. Fotiadis, and A. Engel, 2006. Quantitative dynamic-mode scanning force microscopy in liquid. *Appl. Phys. Lett.* 88:193109–193111.
33. Higgins, M., M. Polcik, T. Fukuma, J. Sader, Y. Nakayama, and S. P. Jarvis, 2006. Structured water layers adjacent to biological membranes. *Biophys. J.* 91:2532–2542.
34. Fukuma, T., A. S. Mostaert, L. C. Serpell, and S. P. Jarvis, 2008. Revealing molecular-level surface structure of amyloid fibrils in liquid by means of frequency modulation atomic force microscopy. *Nanotechnology* 19:384010–384015.
35. Asakawa, H., and T. Fukuma, 2009. The molecular-scale arrangement and mechanical strength of phospholipid/cholesterol mixed bilayers investigated by frequency modulation atomic force microscopy in liquid. *Nanotechnology* 20. 264008-264014.
36. Yamada, H., K. Kobayashi, T. Fukuma, Y. Hirata, T. Kajita, and K. Matsushige, 2009. Molecular resolution imaging of protein molecules in liquid using frequency modulation atomic force microscopy. *Appl. Phys. Express* 2:95007–95009.
37. Nagashima, K., M. Abe, S. Morita, M. Ohta, R. Kokawa, R. Murai, H. Matsumura, H. Adachi, K. Takano, S. M. T. Inoue, and Y. Mori, 2010. Molecular resolution investigation of tetragonal lysozyme (110) face in liquid by frequency-modulation atomic force microscopy. *J. Vac. Sci. Technol. B* 28:C4C11–C4C14.
38. Hoogenboom, B. W., K. Suda, A. Engel, and D. Fotiadis, 2007. The supramolecular assemblies of voltage-dependent anion channels in the native membrane. *J. Mol. Biol.* 370:246–255.
39. Ikegami, K., R. L. Heier, M. Taruishi, H. Takagi, M. Mukai, S. Shimma, S. Taira, K. Hatanaka, N. Morone, I. Yao, P. K. Campbell, S. Yuasa, C. Janke, G. R. MacGregor, and M. Setou, 2007.

- Loss of α -tubulin polyglutamylation in ROSA22 mice is associated with abnormal targeting of KIF1A and modulated synaptic function. *Proc. Natl. Acad. Sci. USA* 104:3213–3218.
40. Konishi, Y., and M. Setou, 2009. Tubulin tyrosination navigates the kinesin-1 motor domain to axons. *Nat. Neurosci.* 12:559–567.
 41. Ikegami, K., and M. Setou, 2010. Unique post-translational modifications in specialized microtubule architecture. *Cell Struct. Funct.* 35:15–22.
 42. Schaap, I. A. T., C. Carrasco, P. J. de Pablo, and D. C. Mackintosh, 2006. Elastic response, buckling, and instability of microtubules under radial indentation. *Biophys. J.* 91:1521–1531.
 43. Munson, K. M., P. G. Mulugeta, and Z. J. Donhauser, 2007. Enhanced mechanical stability of microtubules polymerized with a slowly hydrolyzable nucleotide analogue. *J. Phys. Chem. B.* 111:5053–5057.
 44. Elie-Caille, C., F. Severin, J. Helenius, J. Howard, D. J. Muller, and A. A. Hyman, 2007. Straight GDP-tubulin protofilaments form in the presence of taxol. *Curr. Biol.* 17:1765–1770.
 45. Miller, H. P., and L. Wilson, 2010. Preparation of microtubule protein and purified tubulin from bovine brain by cycles of assembly and disassembly and phosphocellulose chromatography. *Methods Cell Biol.* 95:3–15.
 46. Hamon, L., D. Panda, P. Savarin, V. Joshi, J. Bernhard, E. Mucher, A. Mechulam, P. A. Curmi, and D. Pastré, 2009. Mica surface promotes the assembly of cytoskeletal proteins. *Langmuir* 25:3331–3335.
 47. Thomson, N. H., S. Kasas, B. M. Riederer, S. Catsicas, G. Dietler, A. J. Kulik, and L. Forro, 2003. Large fluctuations in the disassembly rate of microtubules revealed by atomic force microscopy. *Ultramicroscopy* 97:239–247.
 48. Arnal, I., and R. H. Wade, 1999. How does taxol stabilize microtubules? *Curr. Biol.* 5. 900-908.
 49. Markiewicz, P., and M. C. Goh, 1994. Atomic force microscopy probe tip visualization and improvement of images using a simple deconvolution procedure. *Langmuir* 10:5–7.
 50. Wolf, S. G., G. Mosser, and K. H. Downing, 1993. Tubulin conformation in Zinc-induced sheets and microtubules. *J. Struct. Biol.* 111:190–199.

51. Nogales, E., S. G. Wolf, S. X. Zhang, and K. H. Downing, 1995. Preservation of 2-D crystals of tubulin for electron crystallography. *J. Struct. Biol.* 115:199–208.
52. Villasante, A., D. Wang, P. Dobner, P. Dolph, S. A. Lewis, and N. J. Cowan, 1986. Six mouse α -tubulin mRNAs encode five distinct isoforms: Testis-specific expression of two sister genes. *Mol. Cell. Biol.* 6:2409–2419.
53. Sullivan, K. F., and D. W. Cleveland, 1986. Identification of conserved isotype-defining variable region sequences for four vertebrate β tubulin polypeptide classes. *Proc. Natl. Acad. Sci. USA* 83:4327–4331.
54. Luchko, T., J. T. Huzil, M. Stepanovo, and J. Tuszynski, 2008. Conformational analysis of the carboxy-terminal tails of human β -tubulin isoforms. *Biophys. J.* 94:1971–1982.
55. Pal, D., P. Mahapatra, T. Manna, P. Chakrabarti, B. Bhattacharyya, A. Banerjee, G. Basu, and S. Roy, 2001. Conformational properties of α -tubulin tail peptide: Implications for tail-body interaction. *Biochemistry* 40:15512–15519.
56. Boucher, D., J. C. Larcher, F. Gros, and P. Denoulet, 1994. Polyglutamylation of tubulin as a progressive regulator of in vitro interactions between the microtubule-associated protein Tau and tubulin. *Biochemistry* 33:12471–12477.
57. Larcher, J. C., D. Boucher, S. Lazereg, F. Gros, and P. Denoulet, 1996. Interaction of kinesin motor domains with α - and β -tubulin subunits at a Tau-independent binding site. *J. Biol. Chem.* 271:22117–22124.
58. Bonnet, C., D. Boucher, S. Lazereg, B. Pedrotii, K. Islam, P. Denoulet, and J. C. Larcher, 2001. Differential binding regulation of microtubule-associated proteins MAP1A, MAP1B, MAP2 by tubulin polyglutamylation. *J. Biol. Chem.* 276:12839–12848.

Figure Legends

Figure 1.

(a) Size distribution of tubulin structures in the PEM-G buffer solution used in this experiment. (b) FM-AFM image of tubulin protofilaments deposited on mica using the same PEM-G buffer solution ($\Delta f = -10$ Hz, $A = 0.38$ nm, $v = 200$ nm/s).

Figure 2.

(a) FM-AFM image of an isolated tubulin protofilament ($\Delta f = +210$ Hz, $A = 1.44$ nm, $v = 200$ nm/s). (b) Structural model of a tubulin protofilament. Height profiles measured along (c) Lines A-B and (d) Lines C-D shown in (a).

Figure 3.

(a) FM-AFM images of tubulin structures obtained in MES-Zn buffer solution ($\Delta f = +25$ Hz, $A = 0.38$ nm, $v = 300$ nm/s). (b) FM-AFM image of a tubulin sheet-like structure ($\Delta f = 0.0$ Hz, $A = 0.30$ nm, $v = 100$ nm/s). (c) Height profile measured along Line A-B shown in (b). (d) Cutout from (b) as indicated by the dashed line in (b).

Figure 4.

(a) FM-AFM image of a tubulin protofilament in a sheet-like structure ($\Delta f = +3.0$ Hz, $A = 0.30$ nm, $v = 100$ nm/s). (b) Height profile measured along Line A-B shown in (a) (average spacing: 0.53 nm, standard deviation: 0.056, $n=12$). (c) Schematic illustration of α -helix backbone. (d) Structural model of a tubulin heterodimer (PDB ID: 1JFF).

Figure 5.

(a) Cutout from the FM-AFM image shown in Fig. 4(a). The color scale was adjusted to highlight the C-terminal domains. (b) The same image shown with a 21-step color scale. (c) and (d) Schematic illustrations to explain the possible imaging mechanisms of the C-terminal domains.

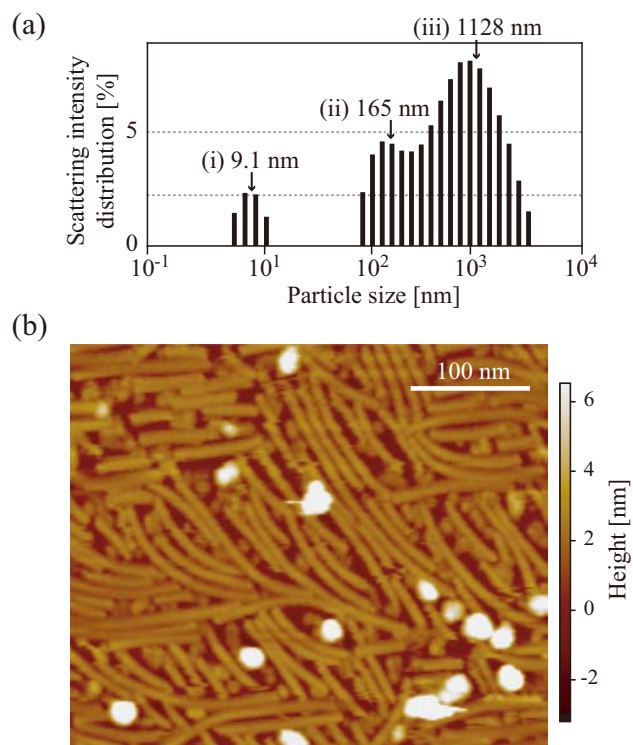


Figure 1:

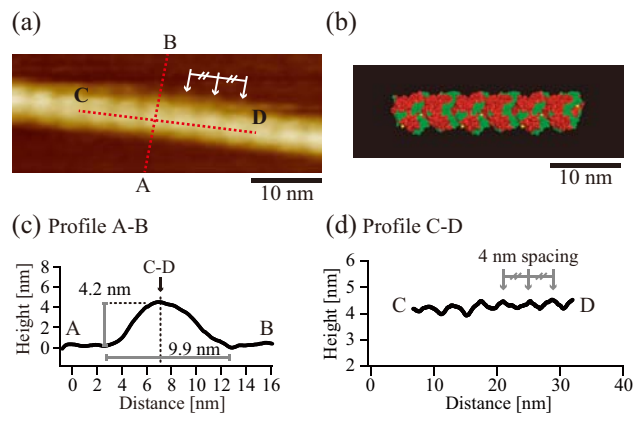


Figure 2:

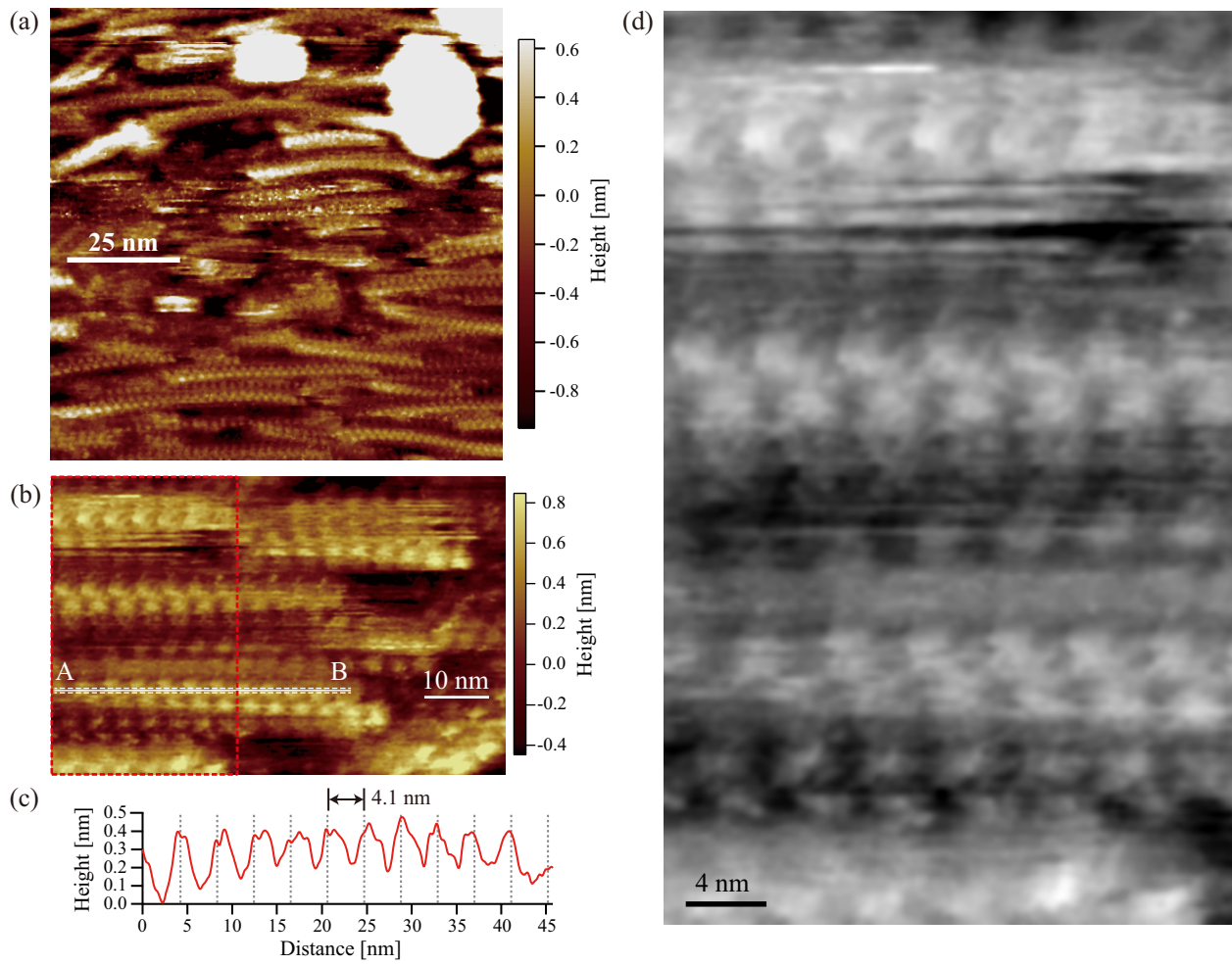


Figure 3:

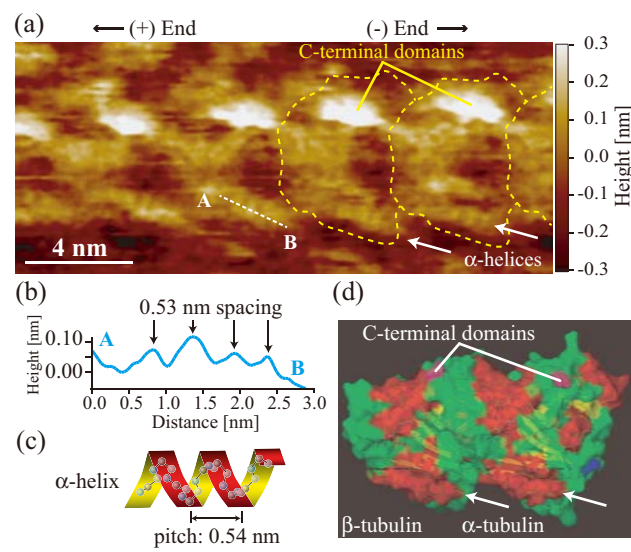


Figure 4:

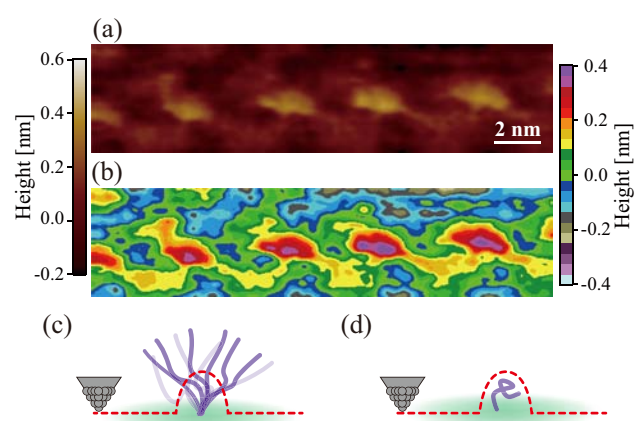


Figure 5: